

1 **Enhanced cellular longevity arising from environmental fluctuations**

2

3 **Authors:** Yuting Liu^{1,†}, Zhen Zhou^{1,†}, Songlin Wu¹, Gavin Ni¹, Alex Zhang¹, Lev S. Tsimring²,

4 Jeff Hasty^{1,2,3}, Nan Hao^{1,2,3*}

5

6 **Affiliations:**

7 ¹Department of Molecular Biology, School of Biological Sciences, University of California San
8 Diego, La Jolla, CA 92093, USA

9 ²Synthetic Biology Institute, University of California San Diego, La Jolla, CA 92093, USA

10 ³Department of Bioengineering, University of California San Diego, La Jolla, CA 92093, USA

11

12

13 *Correspondence to: nhao@ucsd.edu

14 †These authors contributed equally to this work.

15

16

1 **Summary**

2 Cellular longevity is regulated by both genetic and environmental factors. However, the
3 interactions of these factors in the context of aging remain largely unclear. Here, we formulate a
4 mathematical model for dynamic glucose modulation of a core gene circuit in yeast aging, which
5 not only guided the design of pro-longevity interventions, but also revealed the theoretical
6 principles underlying these interventions. We introduce the dynamical systems theory to capture
7 two general means for promoting longevity - the creation of a stable fixed point in the “healthy”
8 state of the cell and the dynamic stabilization of the system around this healthy state through
9 environmental oscillations. Guided by the model, we investigate how both of these can be
10 experimentally realized by dynamically modulating environmental glucose levels. The results
11 establish a paradigm for theoretically analyzing the trajectories and perturbations of aging that
12 can be generalized to aging processes in diverse cell types and organisms.

1 Introduction

2 Aging is driven by accumulation of cellular and genetic damage resulting from intertwined
3 biological processes that are intrinsic to the individual and which are influenced by environmental
4 factors (Lopez-Otin et al., 2013; Mahmoudi and Brunet, 2012; McMurray and Gottschling, 2004;
5 Melzer et al., 2020; Vijg and Suh, 2013). Novel approaches to reduce global healthcare burdens
6 of chronic diseases and aging ultimately demand increased understanding of aging biology and
7 the interactions of the pillars of aging that include diverse yet deeply linked factors such as
8 epigenetics, stress, metabolism, and others (Kennedy et al., 2014; Lopez-Otin et al., 2013).
9 Previous studies in model organisms have been focused on measuring lifespan as a static
10 endpoint assay and have identified many genes, the deletion or overexpression of which affects
11 the lifespan (Fontana et al., 2010; Guarente and Kenyon, 2000; Kaeberlein and Kennedy, 2005;
12 Kenyon, 2010; Kuningas et al., 2008; McCormick et al., 2015). An emerging challenge is to
13 understand how these genes interact with one another and operate collectively to drive the aging
14 processes and determine the final lifespan. Because of the intricacies of aging-related processes,
15 traditional reductionist approaches cannot address the totality of such complexity. Instead, new
16 systems-level approaches that integrate stochastic and nonlinear dynamic models with large time-
17 trace data sets are required.

18 To this end, we set out to quantify and model replicative aging of the budding yeast
19 *Saccharomyces cerevisiae*, a genetically tractable model for aging of mitotic cell types in
20 mammals, such as stem cells. Using microfluidics coupled with time-lapse microscopy
21 (O'Laughlin et al., 2020), we quantitatively tracked the aging processes in a large number of single
22 yeast cells and found that isogenic cells age with two different types of phenotypic changes (Jin
23 et al., 2019; Li et al., 2020; Li et al., 2017; Paxman et al., 2022): about half of cells continuously
24 produced daughters with an elongated morphology during later stages of life (designated as
25 "Mode 1" aging). In contrast, the other half produced small, round daughter cells until death
26 (designated as "Mode 2" aging). Mode 1 aging is driven by ribosomal DNA (rDNA) silencing loss,

1 resulting in dramatically enlarged and fragmented nucleoli, indicating nucleolar decline (Sinclair
2 et al., 1997). In contrast, Mode 2 aging is driven by heme depletion and mitochondrial deterioration
3 (Hughes and Gottschling, 2012).

4 In yeast, the lysine deacetylase Sir2 mediates chromatin silencing at rDNA to maintain the
5 stability of this fragile genomic locus and the integrity of the nucleolus (Gartenberg and Smith,
6 2016; Kaeberlein et al., 1999; Saka et al., 2013; Sinclair and Guarente, 1997). The heme-
7 activated protein (HAP) complex regulates the expression of genes important for heme biogenesis
8 and mitochondrial function (Buschlen et al., 2003). We previously identified a mutual inhibition
9 circuit of Sir2 and HAP that resembles a toggle switch to mediate the fate decision and divergent
10 progression toward Mode 1 vs Mode 2 aging in single cells (Li et al., 2020). Guided by
11 mathematical modeling of the endogenous system, we genetically engineered the Sir2-HAP
12 circuit to reprogram aging trajectories and promote longevity (Li et al., 2020; Zhou et al., 2023).
13 These studies revealed the design principles of genetic circuits for promoting cellular longevity
14 under a static environmental condition. However, how environmental fluctuations impact the
15 dynamical behaviors of genetic circuits to regulate the aging process remains largely unclear.

16 In this study, we used mathematical modeling approach to explore the possibility of
17 rationally reprogramming aging by dynamic environmental inputs. Aging is strongly related to
18 energy metabolism (Bartke et al., 2021; Roberts and Rosenberg, 2006). A growing number of
19 studies revealed that metabolic alterations are a major hallmark of aging, whereas modulating
20 energy metabolism by environmental factors can dramatically influence the phenotypes and rates
21 of aging (Azzu and Valencak, 2017; Jazwinski, 2002; Petr et al., 2021; Ravera et al., 2019). For
22 example, caloric restriction (CR) can promote longevity from yeast to mammals (Al-Regaiey,
23 2016; Arslan-Ergul et al., 2013; Fontana and Partridge, 2015; Hwangbo et al., 2020; Li et al.,
24 2011; Liang et al., 2018; Taormina and Mirisola, 2014). Yet, a systematic, quantitative analysis of
25 the impact of environmental factors on the complex networks of aging remain largely missing,
26 making rational reprogramming of aging a challenging task. To this end, we developed a

1 mathematical model to understand how environmental glucose alterations influence the
2 dynamical behaviors of the core Sir2-HAP circuit and cellular longevity. Based on the single-cell
3 data and dynamical systems theory, we identified two general approaches to extend lifespan by
4 dynamically adjusting environmental glucose inputs - establishing a subtle balance (a stable fixed
5 point) to stabilize the healthy state of the cell and driving dynamic stabilization of the system
6 around this healthy state. Our model not only provides valuable biological insights for designing
7 strategies to promote longevity but also uncovers the underlying theoretical principles behind
8 these strategies, with broad applications across different cell types and organisms.

1 **Results**

2 **Metabolic divergence in isogenic aging cells**

3 To determine how aging affects cellular energy production under standard yeast growth
4 conditions, we monitored cellular ATP levels throughout the lifespans of single cells using a
5 genetically-encoded fluorescent biosensor (Lobas et al., 2019). We observed a gradual decline
6 in cellular ATP levels in Mode 2, but not Mode 1 aging cells (Fig. 1A). To determine the metabolic
7 processes underlying this difference in ATP production among aging cells, we monitored the
8 levels of metabolic factors involved in energy production, such as glycolysis and respiration, and
9 compared their dynamics between Mode 1 and Mode 2 cells.

10 We first examined changes in glycolysis during aging by tracking the expression of
11 glucose transporters (Ozcan and Johnston, 1999), a glycolytic enzyme (Belinchon and Gancedo,
12 2007) and the fluorescence of a fructose-1,6-phosphate (FBP) glycolytic flux biosensor (Monteiro
13 et al., 2019). The three glucose transporters we evaluated (Hxt1, Hxt2, and Hxt3) all showed
14 dramatically increased expression in Mode 2 aging, but only modest changes in Mode 1 aging
15 (Fig. 1B; Fig. S1, A and B), indicating that a marked elevation in glycolysis occurs specifically
16 during Mode 2 aging. Consistent with this observation, the expression of the glycolytic enzyme
17 Hxk1 also increased in Mode 2 but not in Mode 1 aging (Fig. 1C). Moreover, Mode 2 aging cells
18 showed a more dramatic increase in the fluorescence of the glycolytic flux biosensor than Mode
19 1 cells (Fig. S1C). Heme abundance is an indicator of mitochondrial biogenesis and cellular
20 respiration (Buschlen et al., 2003; Zhang et al., 2017). Using a nuclear-anchored infrared
21 fluorescent protein (nuc. iRFP) (Filonov et al., 2011; Li et al., 2020), we tracked heme abundance
22 in single aging cells and observed that it gradually elevated in Mode 1 aging, but dropped sharply
23 in Mode 2 aging (Fig. 1D).

24 Together, these results indicated that Mode 1 aging features an age-induced transition
25 from fermentation to respiration, in agreement with a previous report (Leupold et al., 2019),

1 whereas Mode 2 aging elicits enhanced glycolysis but suppression of respiration, resulting in a
2 decline in ATP production.

3 We next asked if the observed metabolic changes contribute to driving the divergence in
4 Mode 1 and Mode 2 aging or whether they are simply the consequences of different aging routes.
5 We genetically perturbed the glycolysis or respiration pathway and examined the effects on the
6 fate decision in an isogenic aging population (Fig. 1E). We observed that overexpression of the
7 glucose transporter Hxt1 or the glucose sensor Snf3, both of which elevate glucose uptake and
8 glycolysis (Ozcan and Johnston, 1999), promoted Mode 2 aging, whereas deletion of Snf3
9 promoted Mode 1 aging. In addition, overexpression of Hap4, which is a major component of the
10 HAP complex – the master transcriptional activator of yeast respiration (Forsburg and Guarente,
11 1989; Zhang et al., 2017), largely promoted Mode 1 aging, whereas deletion of Hap4 promoted
12 Mode 2 aging, as previously reported (Li et al., 2020). These results demonstrate that metabolic
13 alterations actively regulate the fate decision of single-cell aging – enhancing respiration or
14 reducing glycolysis promotes Mode 1 aging, whereas elevating glycolysis or reducing respiration
15 promotes Mode 2 aging.

16

17 **An optimal level of caloric restriction (CR) for lifespan extension**

18 Environmental glucose levels can modulate metabolic processes, such as glycolysis and
19 respiration (Johnston, 1999; Rolland et al., 2002). To systematically determine how alterations in
20 glucose levels influence the fate decision in aging and the cellular lifespan, we switched the cell
21 growth medium from the standard 2% glucose condition to different glucose levels at the
22 beginning of aging and tracked the lifespans of single cells (Fig. 2; Materials and Methods).

23 We observed that changing glucose levels dramatically affected the fate decision in aging
24 – decreased glucose promoted Mode 1 aging, whereas increased glucose promoted Mode 2
25 aging; the glucose level negatively correlated with the proportions of Mode 1 vs Mode 2 in an

1 aging population (Fig. 2A). However, the average lifespans within Mode 1 and Mode 2 aging cells
2 remained relatively unchanged (Fig. 2B). The exception was with 0.1% glucose, which markedly
3 extended the lifespans of both Mode 1 and Mode 2 aging cells. Further decreasing the glucose
4 level to 0.02%, however, largely shortened the lifespan of Mode 1 cells (>90% of the population).
5 As a result, 0.1% glucose appeared to be an optimal level of CR that maximally extended the
6 lifespan in yeast (Fig. 2C; Lifespan curves and t-tests are included in Fig. S2).

7 To further define the lifespan-extending effect of the optimal CR conditions, we monitored
8 rDNA silencing loss and heme depletion, two major age-induced deterioration processes that
9 regulate lifespan (Li et al., 2020; Zhou et al., 2023). To track rDNA silencing, we used a GFP
10 reporter inserted within the rDNA (rDNA-GFP) (Li et al., 2017). Because expression of the reporter
11 is subject to silencing, increased reporter fluorescence indicates reduced silencing, whereas
12 decreased fluorescence indicates enhanced silencing. To track heme biogenesis, we used a
13 nuclear-anchored iRFP reporter (nuc. iRFP) (Filonov et al., 2011). Its fluorescence depends on a
14 heme degradation product, biliverdin, and thereby correlates with cellular heme levels (Li et al.,
15 2020). We observed that, under the standard 2% glucose condition, about half of cells aged in
16 Mode 1 with decreased rDNA silencing (as indicated by increased rDNA-GFP signal) and
17 increased heme biogenesis (as indicated by increased iRFP signal) at late stages of aging,
18 whereas the other half aged in Mode 2, with decreased heme abundance and modestly changed
19 rDNA silencing (Fig. 2D, top), consistent with previous reports (Li et al., 2020; Zhou et al., 2023).

20 In contrast, in 0.1% glucose, the majority (82%) of cells exhibited Mode 1 aging, but these
21 cells showed a substantial time delay in the loss of rDNA silencing and elevation of heme
22 biogenesis (Fig. 2D, middle), compared to Mode 1 cells in 2% glucose. Decreasing the glucose
23 level to 0.02% further increased the proportion of Mode 1 aging cells (91%). However, we
24 observed an earlier occurrence of age-induced rDNA silencing loss and heme elevation (Fig. 2D,
25 bottom), compared to Mode 1 cells in 0.1% glucose, in accord with a shorter lifespan under this
26 condition. These results suggest that the maximal lifespan extension under 0.1% glucose could

1 be attributed, at least partially, to the time delay in rDNA silencing loss and heme elevation during
2 aging.

3

4 **The emergence of a “longevity fixed point” by CR**

5 To quantitatively analyze mechanisms underlying the emergence of an optimal CR
6 condition, we expanded a recently proposed model, comprising the mutual inhibition circuit of Sir2
7 and HAP that resembles a toggle switch to drive the fate decision in yeast aging (Li et al., 2020).
8 Previous studies revealed that CR can elevate the levels of both Sir2 and HAP in yeast (Anderson
9 et al., 2003; DeRisi et al., 1997; Lin et al., 2002; Medvedik et al., 2007; Westholm et al., 2008).
10 To incorporate these effects in the model, the total amounts of Sir2 and HAP were considered as
11 the functions of the glucose level (Fig. 3, A and B). Thus,

12

$$13 \quad \frac{dS}{dt} = \alpha_1 \left(\beta_1 + \frac{S^{n_1}}{K_S^{n_1} + S^{n_1}} \right) (S_{total}(D) - S) - (d_S + \gamma_1 H) S \quad (1)$$

14

$$15 \quad \frac{dH}{dt} = \alpha_2 \left(\beta_2 + \frac{H^{n_2}}{K_H^{n_2} + H^{n_2}} \right) (H_{total}(D) - H) - (d_H + \gamma_2 S) H \quad (2)$$

16

17 Here, S , H are concentrations of Sir2 and HAP, respectively; α_1 , α_2 are maximum
18 production rates for the positive feedback loop of Sir2 and HAP; β_1 , β_2 are basal activation factors
19 of Sir2 and HAP; K_S , K_H are half-activation constants of Sir2 and HAP; d_S , d_H are degradation
20 rates of Sir2 and HAP; γ_1 , γ_2 are repressive strength of HAP and Sir2; n_1 , n_2 are Hill coefficients
21 for Sir2 and HAP autoregulation. Total capacity of Sir2 and HAP are defined as piecewise
22 functions of glucose concentration D :

23

$$24 \quad S_{total}(D) = \begin{cases} k_{S1}D + b_{S1}, & 0.02 \leq D < 0.1 \\ k_{S2}D + b_{S2}, & 0.1 \leq D < 0.5 \\ k_{S3}D + b_{S3}, & 0.5 \leq D < 2 \\ k_{S4}D + b_{S4}, & 2 \leq D \leq 5 \end{cases} \quad (3)$$

25

$$H_{total}(D) = \begin{cases} k_{H1}D + b_{H1}, & 0.02 \leq D < 0.1 \\ k_{H2}D + b_{H2}, & 0.1 \leq D < 0.5 \\ k_{H3}D + b_{H3}, & 0.5 \leq D < 2 \\ k_{H4}D + b_{H4}, & 2 \leq D \leq 5 \end{cases} \quad (4)$$

2

3 The parameters of the model were estimated by fitting the simulations with the data on the
4 ratios of Mode 1 vs Mode 2 under different glucose conditions (Table S4).

5 To study the stochastic dynamics of aging, we used the following Langevin equations by
6 adding noise terms to the deterministic equations:

7

$$\frac{dS}{dt} = \alpha_1 \left(\beta_1 + \frac{S^{n_1}}{K_S^{n_1} + S^{n_1}} \right) (S_{total}(D) - S) - (d_S + \gamma_1 H) S + S \xi_S \quad (5)$$

9

$$\frac{dH}{dt} = \alpha_2 \left(\beta_2 + \frac{H^{n_2}}{K_H^{n_2} + H^{n_2}} \right) (H_{total}(D) - H) - (d_H + \gamma_2 S) H + H \xi_H \quad (6)$$

11

12 The noise terms ξ_S, ξ_H are uncorrelated white Gaussian processes with zero mean and
13 autocorrelation $\langle \xi_i(t) \xi_i(t') \rangle = \epsilon_i \delta(t - t')$; $i \in \{H, S\}$, where $\delta(t - t')$ is Dirac's delta function and
14 ϵ_i is the magnitude of i .

15 The effects of glucose levels on the dynamics of Sir2 and HAP can be analyzed graphically
16 by plotting the nullclines and vector field in a Sir2-HAP phase plane under different concentrations
17 of glucose (Fig. 3, C and D; Movie S1). With the standard 2% glucose level, the system has two
18 stable fixed points – the low Sir2, high HAP point that corresponds to the terminal state of Mode
19 1 aging and the high Sir2, low HAP point that corresponds to the terminal state of Mode 2 aging
20 (Fig. 3, C and D, top). Stochastic simulations showed that roughly equal numbers of cells
21 progressed toward either of these two steady states during aging (Fig. 3E, top). When the glucose
22 concentration decreases, an unstable fixed point between the two stable fixed points moves
23 toward the high Sir2, low HAP region, biasing the fate decision toward the low Sir2, high HAP
24 state and thereby Mode 1 aging (Movie S1). A third stable fixed point emerges in the intermediate

1 Sir2, intermediate HAP region of the phase plane when the glucose concentration reaches a
2 certain level (Fig. 3, C and D, middle). Stochastic simulations showed that a large fraction of cells
3 fluctuated around this new stable fixed point for a period of time before eventually deviating to the
4 low Sir2, high HAP or high Sir2, low HAP states, driven by the noise (Fig. 3E, middle). These
5 fluctuations are in accord with the delayed rDNA silencing loss and heme elevation observed
6 experimentally under the optimal CR condition (0.1% glucose) (Fig. 2D, middle). This new stable
7 fixed point requires a subtle balance between Sir2 and HAP and hence disappears quickly when
8 the glucose concentration is further decreased (Fig. 3, C and D, bottom). As a result, at 0.02%
9 glucose, the majority of cells aged with Mode 1 aging and rapidly approached the low Sir2, high
10 HAP state (Fig. 3E, bottom), consistent with the aging dynamics observed under this condition
11 (Fig. 2D, bottom).

12 To simulate the effects of glucose alterations on lifespan, we linked the Sir2-HAP circuit
13 to cell death using a paradigmatic model framework recently developed by Uri Alon's group (Karin
14 et al., 2019; Yang et al., 2023), in which the aging process is described as a competition between
15 accelerating damage accumulation and saturating damage removal. The cell death occurs when
16 the level of intracellular damage exceeds a certain threshold value. In our model, we assume that
17 the damage removal rate is dependent on the levels of Sir2 and Hap4. Specifically, the equation
18 for the damage ψ is written as follows:

19

$$20 \quad \frac{d\psi}{dt} = \eta t - \frac{S^2}{S^2 + K_1^2} \frac{H^2}{H^2 + K_2^2} \psi + \psi \xi_\psi \quad (7)$$

21

22 Here, η is the production rate of damage and ξ_ψ is Gaussian white noise term with
23 strength ϵ_ψ . Initial conditions for Sir2 and HAP follow a Gaussian probability distribution

$$24 \quad (2\pi\sigma_S\sigma_H)^{-1} \exp\left[-\frac{(S-S_0)^2}{\sigma_S^2} - \frac{(H-H_0)^2}{\sigma_H^2}\right] \text{ (see Table S4 for the parameters of simulations).}$$

1 Decreasing either Sir2 or HAP levels reduces damage repair/removal and thereby
2 accelerates damage accumulation. The lifespan of a cell is calculated as the time taken for its
3 damage level to hit the threshold (Fig. 3F). The optimal CR condition allows for the system to
4 spend an extended period near the new stable fixed point with intermediate Sir2 and HAP levels
5 and hence to slow damage accumulation, leading to the maximally extended lifespan across
6 different glucose levels (Fig. 3G). We therefore designated this stable fixed point as a “longevity
7 fixed point.”

8

9 **Sir2 overexpression can stabilize the longevity fixed point**

10 To determine the dependence of the longevity fixed point on the glucose concentration,
11 we performed a bifurcation analysis of our model (Equations 5 and 6) and showed that, in the WT
12 system, the longevity fixed point emerges within a narrow range of glucose levels, into which the
13 optimal CR falls (Fig. 4A, left). Consistently, in WT, the longevity fixed point only exists within a
14 small triangular region of the Sir2-HAP parameter space and the trajectory depicting glucose level
15 changes passes across only the tip of that region (Fig. 4A, right).

16 Our previous analysis of the Sir2-HAP model revealed that 2-fold overexpression of Sir2
17 can also create the longevity fixed point under standard growth conditions (corresponding to long-
18 lived Mode 3 aging) (Li et al., 2020). We therefore examined how Sir2 overexpression can alter
19 the dependence of this fixed point on glucose levels. Our model predicted that increasing Sir2
20 abundance by 2-fold (see Materials and Methods) can reshape the phase diagram of the system
21 so that the longevity fixed point can exist within a much wider range of glucose levels and a larger
22 region of the Sir2-HAP parameter space (Fig. 4B).

23 In addition, because the two flanking unstable fixed points are moved further away from
24 the longevity fixed point by Sir2 overexpression, the system becomes less likely to deviate to the
25 other two “aged” stable fixed points by the noise (Fig. 4, C and D), which could lead to longer
26 lifespans under a wide range of glucose levels, compared to that of WT cells under the optimal

1 CR condition. Changing the glucose level can still modulate the distances between the longevity
2 fixed point and the two flanking unstable fixed points and thereby can influence the fate decision
3 in the 2 x Sir2 system: 2% glucose biased the system toward deviation to the high Sir2, low HAP
4 state and Mode 2 aging, whereas 0.02% glucose biased the system toward the low Sir2, high
5 HAP state and Mode 1 aging; 0.1% glucose remained the optimally balanced condition with the
6 least chance of deviations.

7 To test these predictions experimentally, we overexpressed Sir2 by 2-fold and monitored
8 cell aging under different glucose concentrations. Consistent with the model, we observed
9 substantially delayed rDNA silencing loss and heme elevation in a large fraction of cells under all
10 the tested glucose concentrations (0.02% - 3%) (Fig. 4E), which resulted in longer lifespans than
11 that of WT cells over a wide range of glucose levels (Fig. 4F; lifespan curves and t-tests are
12 included in Fig. S3). These results are in accord with a more stable longevity fixed point in the 2
13 x Sir2 system. In addition, glucose levels can indeed affect the fate decisions of aging cells with
14 Sir2 overexpression (Fig. 4E), consistent with model simulations (Fig. 4D).

15

16 **External glucose oscillations can enable “dynamic stabilization” of the aging** 17 **process**

18 We recently engineered a synthetic Sir2-HAP gene oscillator that could slow cell
19 deterioration, resulting in a dramatically extended lifespan (Zhou et al., 2023). In this study we
20 considered the possibility that oscillatory glucose inputs may be able to drive dynamic stabilization
21 of the Sir2-HAP circuit and thereby promote longevity. For example, in our model, the system
22 does not have the longevity fixed point at either 2% or 0.02% glucose levels and is unstable in
23 the intermediate Sir2, intermediate HAP range. However, oscillations between 0.02% and 2%
24 glucose levels may be able to restrict the system to that region, reaching a state of dynamic
25 stabilization.

1 To test this possibility *in silico*, we first performed stochastic simulations with external
2 glucose oscillations between 0.02% and 2%. We found that at least a fraction of cells indeed
3 remains within the intermediate Sir2, intermediate HAP state for an extended period before
4 escaping to the low Sir2 or low HAP states (Fig. 5, A-C; Movie S2). Increasing the frequency of
5 glucose oscillations increases the proportion of cells that exhibit such a delay (Fig. 5D; Fig. S4).

6 To determine whether this delay depends on the existence of the stable longevity fixed
7 point at the constant 0.1% glucose condition, we modified the dependence functions of Sir2 and
8 HAP on the glucose level, $S_{total}(D)$ and $H_{total}(D)$, so that the longevity fixed point would never
9 emerge in the system at any glucose level (Fig. S5A). We found that external glucose oscillations
10 can still generate an extended delay before fate commitments (Fig. S5B), indicating that the
11 dynamic stabilization does not require the presence of the stable longevity fixed point at an
12 intermediate level of glucose. The mechanistic reason for the emergence of the delay is that
13 oscillations between two different levels of glucose lead to an averaging effect of the two
14 corresponding states in the (S_{total}, H_{total}) parameter space and this novel averaged state
15 features a stable fixed point for longevity (Fig. S5A). These modeling results suggest that
16 oscillatory external inputs can enable dynamic stabilization of Sir2 and HAP levels within an
17 optimal range and thereby extend lifespan.

18 To test these computational predictions experimentally, we integrated our microfluidic
19 device with a computer-controlled electrovalve (Hansen et al., 2015; Hersen et al., 2008) to deliver
20 dynamic patterns of environmental inputs into the culture chambers. We applied external glucose
21 oscillations between 0.02% and 2% with 6-hour period throughout the lifespans of yeast cells and
22 tracked their aging processes. In addition to Mode 1 and Mode 2 aging cells, we observed that
23 about one-third of cells showed fluctuating rDNA-GFP and iRFP signals for a long period of time
24 before deviating to the low HAP state (Fig. 5E). These cells corresponded to the fraction of cells
25 with dynamic stability in our model simulations. We hence designated them as dynamically

1 stabilized (DS) cells. These DS cells turned out to be very long-lived, with an average lifespan of
2 35 generations, much longer than that of Mode 1 or Mode 2 cells from the same aging population
3 (Fig. 5F). We further tested glucose oscillations with an input period of 12 hours and 24 hours.
4 Consistent with model simulations, decreasing the input frequency reduced the proportion of
5 Mode DS cells in an aging population (Fig. 5G).

6 Taken together, these results validated our modeling results and demonstrated that
7 external glucose oscillations can indeed enable dynamic stabilization of aging processes, leading
8 to a prolonged lifespan.

9

1 Discussion

2 In this study, we devised a simple mathematical model that can not only reproduce the
3 single-cell aging data under variable glucose conditions but also shed light on the underlying
4 biological mechanisms governing the metabolic regulation of aging. Importantly, the model has
5 predictive power that can be used to guide the design of interventional strategies for longevity
6 and to reveal the theoretical principles underlying these strategies. In particular, we focused on
7 the Sir2-HAP toggle switch circuit that mediates the progression of two major aging paths in single
8 yeast cells – one leads to a low Sir2, high HAP state, resulting in nucleolar decline, and the other
9 leads to a high Sir2, low HAP state, causing mitochondrial deterioration (Fig. 3) (Li et al., 2020).
10 Because both of these terminal states of aging are associated with markedly accelerated damage
11 accumulation, the overall goal for pro-longevity interventions is to avoid, or at least delay, the fate
12 commitment and progression toward these two detrimental steady states (stable fixed points) of
13 the natural aging system. This is challenging in that interventions that elevate either end of the
14 toggle, Sir2 or HAP, will simply push the cell to the other path toward aging and death.

15 Our model-based analysis here unraveled two general approaches to promote longevity:
16 (1) create and stabilize a new longevity fixed point in the “healthy” intermediate Sir2 and HAP
17 region; and (2) enable dynamic stabilization of the system around the “healthy” state. Both can
18 be realized by dynamically modulating environmental glucose levels.

19 For the first approach, the longevity fixed point, which achieves a subtle balance between
20 Sir2 and HAP at intermediate levels, can be stabilized by either an optimal level of CR or moderate
21 overexpression of Sir2. Both interventions enable the cell to maintain a state with intermediate
22 levels of Sir2 and HAP for an extended period of time. Among them, genetic manipulation of Sir2
23 leads to a fixed point that is less sensitive to environmental glucose alterations (Fig. 4B).
24 Intriguingly, however, although Sir2 overexpression and CR extend the lifespan through the same
25 mechanism, their effects can still be additive (Fig. 4F). The glucose level, by acting on HAP as
26 well as Sir2, can modulate the stability of the longevity fixed point generated by Sir2

1 overexpression and thereby influence the lifespan (Fig. 4D). As an immediate application, our
2 model can be used to design the combined treatments with CR and pharmacological activators
3 of sirtuins, in which *in silico* simulations could help refine the optimal dosage combinations for
4 maximizing the effects on lifespan extension.

5 For the second approach inspired by the nonlinear dynamics and control theory, we
6 adopted the concept of dynamic stabilization for designing pro-longevity strategies. Indeed, an
7 unstable state of a dynamical system, such as the natural aging circuit with intermediate levels of
8 Sir2 and HAP, can be stabilized by applying periodic oscillations of external glucose levels at
9 certain frequencies (Fig. 5, A and B). More generally, it is possible that oscillatory inputs can
10 stabilize the system in a healthy, long-lived state whereas the constant inputs cannot (Fig. 5C). It
11 is interesting to note that this method of dynamical stabilization is reminiscent of the stabilization
12 of inverted pendulum by periodic vibrations of its pivot point, so-called Kapitza's pendulum
13 (Blackburn, 1992). Tuning the frequency can modulate the strength of this dynamic stabilization
14 and thereby the proportion of cells that age through this long-lived state of unstable equilibrium
15 (Fig. 5D).

16 Temporally-varying metabolic interventions, such as intermittent fasting, are attracting
17 increasing attention as a potential approach to effectively promote longevity and healthspan
18 (Fontana and Partridge, 2015; Hwangbo et al., 2020; Longo and Panda, 2016; Mattson et al.,
19 2017), but definition of mechanisms underlying their effectiveness remain elusive. Our dynamic
20 stabilization theory of aging, validated here in yeast, may provide the theoretical underpinning for
21 the effects of temporally-varying interventions. As large-scale intervention testing is prohibitively
22 time- and resource-intensive, models based on this theoretical framework can help screen and
23 identify *in silico* the optimal dynamic patterns of metabolic interventions for experimental
24 examinations. Such model-directed approaches can also be applied to identify time-based
25 administration regimes for a series of metabolic intervention compounds named "caloric restriction
26 mimetics" (CRM), including rapamycin, metformin, and spermidine, shown to increase lifespan in

1 multiple model organisms (Barzilai et al., 2016; Madeo et al., 2019; Madeo et al., 2018; Martel et
2 al., 2021; Miller et al., 2011; Mohammed et al., 2021; Novelle et al., 2016; Selvarani et al., 2021).

3 In addition to the two approaches presented here, a third approach, creating a limit cycle
4 for longevity, was conceived by attempts to modify the circuit structure in the model. Rewiring the
5 mutual inhibition between Sir2 and HAP into a negative feedback loop can replace the detrimental
6 stable fixed points with a limit cycle on the Sir2-HAP phase plane, leading to sustained oscillations
7 in Sir2 and HAP levels and thereby avoiding fate commitment to either low Sir2 or low HAP state.
8 This strategy has been realized by genetic circuit engineering in the cell (Zhou et al., 2023).

9 Our model is designed specifically for yeast aging, yet due to its abstract nature, it can be
10 readily applied to design interventions for any fate decision processes driven by toggle switch
11 circuits, such as trophectoderm differentiation by the Oct3/4-Cdx2 circuit (Niwa et al., 2005),
12 induced pluripotent stem cell reprogramming by the Oct4-Sox2 circuit (Shu et al., 2013),
13 hematopoietic stem cell differentiation by the GATA-1 and PU.1 circuit (Liew et al., 2006), and
14 many others. Future studies will be focused on identifying major toggle switch circuits that drive
15 aging in other organisms or in human cells, based on which we can apply our modeling framework
16 to design and test universal interventional strategies for promoting longevity.

17

18

19

1 **Acknowledgements**

2 We thank Dr. Lorraine Pillus for insightful discussions and suggestions on the manuscript. This
3 work was supported by National Institutes of Health R01AG056440 (to N.H., J.H., L.S.T.),
4 R01GM144595 (to N.H., J.H., L.S.T.), R01GM111458 (to N.H.) and R01AG068112 (to N.H.).

5

6 **Author Contributions**

7 Conceptualization, Y.L., Z.Z., L.S.T., J.H., and N.H.; Methodology, Y.L., Z.Z., L.S.T., J.H., and
8 N.H.; Investigation, Y.L., Z.Z., S.W., G.N., A.Z.; Formal Analysis, Y.L., Z.Z., S.W., L.S.T.; Writing
9 - Original Draft, Y.L., Z.Z., and N.H.; Writing - Review & Editing, Y.L., Z.Z., S.W., G.N., A.Z., L.S.T.,
10 J.H., and N.H.; Resources, L.S.T., J.H., and N.H.; Supervision, N.H.; Funding Acquisition, L.S.T.,
11 J.H., and N.H.

12

13 **Declaration of Interests**

14 The authors declare no competing interests.

15

1 **Figure legends**

2 **Fig 1. Distinct metabolic changes in Mode 1 vs Mode 2 aging. (A-D)** Dynamics of an ATP
3 reporter (A, n=116), Hxt3-mCherry (B, n=119), Hxk1-GFP (C, n=115), nuc. iRFP (D, n = 120) in
4 Mode 1 and Mode 2 cells. (Top left of each panel) Representative time-lapse images of single
5 Mode 1 and Mode 2 cells. Mother cells are circled in yellow, and the replicative age of the mother
6 cell is shown at the top left corner of each image. (Bottom left of each panel) Single-cell color map
7 trajectories in Mode 1 and Mode 2 cells. Each row represents the time trace of a single cell
8 throughout its lifespan. Color represents the fluorescence intensity as indicated in the color bar.
9 (Right of each panel) Average fluorescence time traces throughout the life spans in Mode 1 and
10 Mode 2 cells. **(E)** Effects of metabolic gene perturbations on the fate decision in yeast aging. Pie
11 charts show the percentages of Mode 1 (red) and Mode 2 (blue) in WT and mutants tested. O/E:
12 overexpression.

13
14 **Fig 2. The effects of glucose levels on aging and lifespan. (A)** The percentage of Mode 1 cells
15 in an aging population as a function of glucose concentration. **(B)** The average lifespans of Mode
16 1 and Mode 2 cells as a function of glucose concentration **(C)** The average lifespan of a whole
17 aging population as a function of the glucose level. Lifespan curves and statistical analysis are
18 shown in Fig. S2. **(D)** Single-cell color map trajectories of rDNA-GFP (left) and nuclear-anchored
19 iRFP (right) during aging under different glucose levels (2% Glucose: n = 91; 0.1% Glucose: n =
20 80; 0.02% Glucose: n = 100). Each row represents the time trace of a single cell throughout its
21 life span. Color represents the fluorescence intensity as indicated in the color bar. Color maps for
22 rDNA-GFP and nuc. iRFP are from the same cells with the same vertical order. For each glucose
23 level, cells are classified into Mode 1 (top) and Mode 2 (bottom) based on their aging phenotypes
24 and reporter dynamics.

25

1 **Fig. 3. Computational modeling unravels the stability changes of the Sir2-HAP circuit**
2 **under different glucose levels. (A)** Diagram of the circuit topology. **(B)** Equations of the model.
3 S is the concentration of enzymatically active Sir2, H is the concentration of active HAP complex
4 and D is the concentration of glucose. S_{total} and H_{total} are piecewise functions of D , representing
5 the total concentration of Sir2 and HAP, respectively (see Methods for details). **(C)** Phase planes
6 demonstrate the stability changes of the Sir2-HAP circuit under different glucose levels. The
7 nullclines of Sir2 and HAP are represented in blue and red, respectively. The arrows represent
8 the rate and direction of the system's movement. Fixed points are indicated with open (unstable)
9 and closed (stable) circles. The stable fixed point at the top left corner of each phase plane
10 corresponds to the terminal state of Mode 1 aging and the one at the bottom right corner
11 corresponds to the terminal state of Mode 2 aging. At 0.1% glucose, a third stable fixed point
12 ("longevity fixed point") emerges with intermediate levels of Sir2 and HAP. **(D)** Stochastic
13 simulations of aging trajectories on the Sir2-HAP phase planes under different glucose levels.
14 The initial points of each trajectory (purple, $n=10$) were randomly generated based on the
15 Gaussian distribution for simulation. Trajectories were numerically calculated by the stochastic
16 version of equations from (B). **(E)** Stochastic simulations of the Sir2 and HAP time traces during
17 aging under different glucose levels. The initial points ($n=200$) were randomly generated based
18 on the Gaussian distribution for simulation. Red and blue curves represent the time traces of
19 Mode 1 and Mode 2 cells, respectively. **(F)** Simulated time traces of damage accumulation based
20 on Sir2 and HAP dynamics in (E). The cell is considered "dead" once its damage level exceeds
21 the arbitrary threshold (horizontal line). **(G)** Simulated lifetime as a function of the glucose
22 concentration. Simulations were performed 5 times with 100 cells for each simulation. The black
23 dots and error bars represent the mean value and standard deviation of simulated lifetimes,
24 respectively.
25

1 **Fig. 4. Sir2 overexpression stabilizes the longevity fixed point. (A-B)** Dependence of the
2 longevity fixed point on the glucose level in WT and 2xSir2. (A-B, left) Bifurcation analysis for the
3 stability of the Sir2-HAP circuit as a function of the glucose level. Black lines and grey lines
4 represent stable and unstable fixed points, respectively. The range of glucose levels in which the
5 longevity fixed point exists is shaded in blue. (A-B, right) The dependence of the longevity fixed
6 point on the total amounts of Sir2 (S_{total}) and HAP (H_{total}). The glucose level can affect the values
7 of S_{total} and H_{total} , which is depicted by the red line. The blue region represents the area where the
8 longevity fixed point exists in the parameter space. (C) The Sir2-HAP phase planes for 2xSir2
9 under different glucose levels. (D) Stochastic simulations of aging trajectories on the Sir2-HAP
10 phase planes for 2xSir2 under different glucose levels. (E) Single-cell color map trajectories of
11 rDNA-GFP (left) and nuc. iRFP (right) for cells with 2-fold overexpression of *SIR2* under different
12 glucose conditions (2% glucose: n = 53; 0.1% glucose: n = 50; 0.02% glucose: n = 41). (F) The
13 experimentally-measured lifespans of WT vs 2xSir2 as a function of the glucose level.

14

15 **Fig. 5. External glucose oscillations enable dynamic stabilization of the aging process. (A)**
16 Stochastic simulations of the Sir2 and HAP time traces during aging under glucose oscillations
17 between 0.02% and 2%, with a 6-hr period (n=200). Dynamically stabilized (DS) cells were
18 defined as those that continue to fluctuate around the intermediate Sir2 and HAP state for an
19 extended period before deviation to Mode 1 or Mode 2 (see Material and Methods). The time
20 traces of DS cells are shown in purple. (B) Simulated time traces of damage accumulation based
21 on Sir2 and HAP dynamics in (A). The cell is considered “dead” when its damage level exceeds
22 the arbitrary threshold (horizontal line). (C) Stability of aging trajectories upon glucose oscillations
23 vs constant glucose levels. Stochastic simulations were performed in a Sir2-HAP plane of
24 200×200 grids, and the average retention probability in each grid was computed, as indicated by
25 the color bar. (D) The percentage of DS cells in an aging population as a function of the period of
26 glucose oscillations, from model simulations. (E) Single-cell color map trajectories of rDNA-GFP

1 (left) and nuc. iRFP (right) during aging under glucose oscillations between 0.02% and 2% with a
2 period of 6 hours (n=84). Each row represents the time trace of a single cell throughout its life
3 span. Color represents the fluorescence intensity as indicated in the color bar. Color maps for
4 rDNA-GFP and nuc. iRFP are from the same cells with the same vertical order. Under each
5 glucose level, cells are classified into Mode 1 (top), Mode 2 (middle) and DS (bottom) based on
6 their aging phenotypes and reporter dynamics. **(F)** Lifespan curves of Mode 1, Mode 2, and DS
7 cells. **(G)** The percentage of DS cells in an aging population as a function of the period of glucose
8 oscillations, determined by experiments.

9
10

1 **Materials and Methods**

2 ***Strain and plasmid construction***

3 Standard protocols were used for molecular cloning. All yeast strain used in this study
4 were constructed based on BY4741 (*MATa his3Δ1 leu2Δ0 met15Δ0 ura3Δ0*). Details of strains,
5 plasmids, and primers are included in Table S1-S3.

6 To make the *SIR2* 2-fold overexpression plasmid, a *XbaI*_p*SIR2*_SIR2_*EcoRI* fragment
7 containing 620 bp of the *SIR2* promoter + the *SIR2* ORF was made by PCR and then ligated into
8 pRS303, yielding plasmid NHB0638.

9 To make the plasmid for the ATP reporter, a DNA fragment containing sequences from
10 iATPSnFR^{1.0} (including epsilon subunit, Linkers 1 and 2, GFP sequences) (Lobas et al., 2019)
11 was synthesized by IDT with codon optimization for yeast BY4741. Then PCR and Gibson
12 Assembly were used to insert the 408bp *TEF1* promoter and the iATPSnFR^{1.0} fragment into
13 pRS303 plasmid, yielding NHB1222.

14 To make the plasmid for glycolysis (FBP) reporter, pHO_pTEFmut7_CggR_R250A_ble
15 (#124585) and pCggRO-reporter (#124582) plasmids were purchased from Addgene (Monteiro
16 et al., 2019). Then forward primer with BamHI cutting site and reverse primer with EcoRI cutting
17 site were used to PCR CggRO sequence. Forward primer with XhoI cutting site and reverse
18 primer with EcoRI cutting site were used to PCR pTEFmut7_CggR_R250A sequences. After that,
19 the two PCR fragments were ligated into pRS303 plasmid cut by XhoI and BamHI to get the
20 plasmid NHB1227.

21 The yeast strain with the nuc. iRFP reporter (NH268) and the strain with both nuc. iRFP
22 and the NTS1 silencing reporters (NH270) was made as previously described (Li et al., 2017).
23 The yeast strain with the ATP reporter was made by transforming NH268 with DNA fragments
24 from NHB1222 digested by BsmI. The yeast strain with Hxt1-CFP, Hxt2-YFP, Hxt3-mCherry
25 reporters was made by the following steps: firstly, mCherry-LEU2 was amplified by PCR and
26 integrated at the C-terminus of Hxt3 by homologous recombination to make the Hxt3-mCherry

1 strain; secondly, CFP-HIS3 was amplified by PCR and integrated at the C-terminus of Hxt1 by
2 homologous recombination to make the Hxt3-mCherry, Hxt1-CFP strain; Lastly, YFP-URA3 was
3 amplified by PCR and integrated at the C-terminus of Hxt2 by homologous recombination to make
4 the Hxt3-mCherry, Hxt1-CFP, Hxt2-YFP strain. Similarly, the yeast strain with the Hxk1-GFP
5 reporter was made by transforming GFP-HIS3 fragments amplified from PCR. The yeast strain
6 with the glycolysis reporter was made by transforming NH268 with DNA fragments from NHB1227
7 digested by BsmI.

8
9 ***Setting up microfluidic experiments and time-lapse microscopy***

10 The microfluidic devices and experiments were set up as previously described (Zhou et
11 al., 2023). The yeast cells were incubated in SC medium containing 2% glucose before loading
12 into the microfluidic devices. SC media containing different concentrations of glucose were
13 delivered to cells via the media supply syringes after cell loading and were applied throughout the
14 experiments.

15 A computer-controlled electrovalve was used to deliver external glucose oscillations to
16 aging cells in the microfluidic device. The 3-way 0.054 ports electrovalve (The Lee Company,
17 #LFYA1226032H) was connected to a 4-channel USB powered relay module (Numato Lab, SKU:
18 USBPOWRL004). Each channel of the relay could be programmed to control the media input to
19 one microfluidic device by custom-designed MATLAB App. To generate glucose oscillations,
20 growth media with 2% glucose and 0.02% glucose were connected to Port I and O of the
21 electrovalve, respectively, which can be computer-controlled. The outlet port of the valve was
22 connected to the inlet of the microfluidic device.

23 Time-lapse microscopy experiments were conducted using a Nikon Ti-E inverted
24 fluorescence microscope with an EMCCD camera (Andor iXon X3 DU897). The light source is a
25 spectra X LED system. Images were taken using a CFI plan Apochromat Lambda DM 60X oil
26 immersion objective (NA 1.40 WD 0.13MM). In all experiments, the images were acquired for

1 each fluorescence channel every 15 min for a total of 90 to 120 hours. The exposure and intensity
2 setting for each channel were set as follows: 1) For the glucose tuning assay: Phase 80 ms, GFP
3 4 ms/30ms at 10% lamp intensity with an EM Gain of 70, and iRFP 50 ms at 15% lamp intensity
4 with an EM Gain of 300; 2) For detecting the ATP reporter : Phase 80 ms, GFP 30ms at 10%
5 lamp intensity with an EM Gain of 70, and iRFP 300ms at 15% lamp intensity with an EM Gain of
6 300; 3) For detecting Hxt1-3: Phase 80 ms, mCherry 100ms at 25% lamp intensity with an EM
7 Gain of 250, YFP 100ms at 10% lamp intensity with an EM Gain of 250, CFP 60ms at 10% lamp
8 intensity with an EM Gain of 250 and iRFP 300ms at 15% lamp intensity with an EM Gain of 100;
9 4) For detecting the FBP reporter : Phase 50 ms, YFP 200ms at 10% lamp intensity with an EM
10 Gain of 250, and iRFP 300ms at 15% lamp intensity with an EM Gain of 100.

11

12 ***Quantification of single-cell aging traces***

13 Image processing was conducted using a custom MATLAB code (Li et al., 2020; Li et al.,
14 2017; Zhou et al., 2023). The background of images from each fluorescence channel were
15 subtracted. Cell nuclei were masked by thresholding iRFP signal. The mean intensity value of the
16 top 40% of the pixels of fluorescence reporters was quantified, as described previously (Li et al.,
17 2020; Li et al., 2017; Zhou et al., 2023). The time traces of reporters were smoothed using the
18 MATLAB function *smoothdata* with specification of the Gaussian method through a 15-element
19 sliding window.

20 To plot the cell cycle length changes as a function of the percentage of lifetime, the vector
21 of cell cycle length was interpolated to a new vector of 100 elements at evenly distributed 100
22 query points. For single cell aging dynamics and replicative lifespan (RLS) analyses, we collected
23 data from at least 3 independent experiments. Any cells showing obvious abnormal morphologies
24 upon cell loading were filtered out for RLS analysis. Any cells showing dislocation of reporter
25 mask were filtered out for time trace analysis but included in RLS analysis. Significant numbers

1 for RLS changes were calculated with Gehan-Breslow-Wilcoxon test by using Prism GraphPad 7
2 (GraphPad Software, CA).

3

4 ***Computational Modeling***

5 Stochastic simulations

6 The stochastic dynamics of aging were studied using the following Langevin equations by adding
7 noise terms to the deterministic equations:

$$8 \quad \frac{dS}{dt} = \alpha_1 \left(\beta_1 + \frac{S^{n_1}}{K_S^{n_1} + S^{n_1}} \right) (S_{total}(D) - S) - (d_S + \gamma_1 H) S + S \xi_S \quad (5)$$

$$9 \quad \frac{dH}{dt} = \alpha_2 \left(\beta_2 + \frac{H^{n_2}}{K_H^{n_2} + H^{n_2}} \right) (H_{total}(D) - H) - (d_H + \gamma_2 S) H + H \xi_H \quad (6)$$

10 The noise terms ξ_S, ξ_H are uncorrelated white Gaussian processes with zero mean and
11 autocorrelation $\langle \xi_i(t) \xi_i(t') \rangle = \epsilon_i \delta(t - t')$; $i \in \{H, S\}$, where $\delta(t - t')$ is Dirac's delta and ϵ_i is the
12 magnitude of i .

13 To simulate the lifetime of each cell, we coupled the saturated-repair stochastic equation
14 described by (Yang et al., 2023) with equations (5) & (6). The damage removal term was modified
15 with respect to the level of Sir2 and HAP, the equation is listed as following:

$$16 \quad \frac{d\psi}{dt} = \eta t - \frac{S^2}{S^2 + K_1^2} \frac{H^2}{H^2 + K_2^2} \psi + \psi \xi_\psi \quad (7)$$

17 where η is the maximum production rate of damage, ξ_ψ is a Gaussian white noise term with
18 strength ϵ_ψ . The cell was defined as dead when cellular damage ψ reached the threshold which
19 was set to 5 in our cases. Initial conditions for Sir2 and HAP follow a Gaussian probability
20 distribution $(2\pi\sigma_S\sigma_H)^{-1} \exp \left[-\frac{(S-S_0)^2}{\sigma_S^2} - \frac{(H-H_0)^2}{\sigma_H^2} \right]$ (see Table S4 for the parameters of simulations).

21

22 Bifurcation analysis

1 The fixed points of equation (1) & (2) were calculated by *fsolve* from SciPy. Points with negative
2 values were omitted. The eigenvalues of Jacobian matrix of equations (1) & (2) at fixed point were
3 calculated to determine its stability. The sweet spot (the third stable fixed point) was defined as
4 the point that has both negative eigenvalues and lies within the range of 15%-70% of Sir2 and
5 HAP total amount.

6

7 Mode ratio determination

8 Mode 2 was defined as H equals 0 at the end of simulated lifetime. We defined the number of
9 Mode 1 cell equals $N-M_2$, where the N is the number of overall cells and M_2 is the number of Mode
10 2 cells. The mode ratio equals $\frac{N-M_2}{N}$.

11

12 Mode DS determination

13 To get the distributions of lifetime of Mode 1 and Mode 2 cells, 20,000 rounds of simulation were
14 conducted corresponding to the conditions of 0.02% and 2% glucose, respectively. The lifetimes
15 for Mode 1 and Mode 2 were fitted to gamma distributions separately (Fig. S4). The threshold in
16 each mode for defining “Mode DS” was set as Cumulative Distribution Function (CDF)=95%.

17

18 2 × Sir2 overexpression approximation

19 When another copy of *SIR2* gene was added, total Sir2 capacity was increased by a factor of κ .
20 Equation 5 became:

$$21 \quad \frac{dS}{dt} = \alpha_1 \left(\beta_1 + \frac{S^{n_1}}{K_S^{n_1} + S^{n_1}} \right) (\kappa S_{total}(D) - S) - (d_S + \gamma_1 H)S + S\xi_S \quad (8)$$

22 Considering Sir2 is nicotinamide adenine dinucleotide (NAD⁺)-dependent enzyme,
23 overexpression of Sir2 may lead to competitive binding of NAD⁺, which reduces the inhibition
24 strength (γ_2) to HAP. The assumption is in line with our experimental results in which 2 × Sir2 in
25 2% glucose condition exhibited no effect on pushing the cells to Mode 2 (~57% mode 1 of 2 ×

1 Sir2 vs ~50% mode 1 of WT), indicating a compromise of increase of Sir2 capacity and reduction
 2 of Sir2 activity simultaneously. In addition, an extreme overexpression of Sir2 driven by the strong
 3 promoter, *pTDH3*, leads to almost 100% mode 1 cells. This suggests that Sir2 does not exert an
 4 inhibitory effect on HAP through the loss of Sir2 enzymatic activity, caused by severe competition
 5 for NAD⁺. In this case, we set κ equals 1.2 and γ_2 equals 0.5.

6

Strain Name	Description
NH0268	<i>BY4741 MATa his3Δ1 leu2Δ0 met15Δ0 ura3Δ0, NHP6a-iRFP-kanMX</i>
NH0270	<i>BY4741 MATa his3Δ1 leu2Δ0 met15Δ0 ura3Δ0, RDN1::NTS1-P_{TDH3}-GFP-URA3,NHP6a-iRFP-kanMX</i>
NH0886	<i>BY4741 MATa his3Δ1 leu2Δ0 met15Δ0 ura3Δ0, RDN1::NTS1-P_{TDH3}-GFP-URA3,NHP6a-iRFP-kanMX, pSIR2::pSIR2-SIR2-HIS3</i>
NH1641	<i>BY4741 MATa his3Δ1 leu2Δ0 met15Δ0 ura3Δ0, NHP6a-iRFP-kanMX, HXT3-mCherry::LEU2; HXT1-CFP::HIS3; HXT2-YFP::URA3</i>
NH1692	<i>BY4741 MATa his3Δ1 leu2Δ0 met15Δ0 ura3Δ0, NHP6a-iRFP-kanMX, pTEF1-iATPSnFR1.0::HIS3</i>
NH1704	<i>BY4741 MATa his3Δ1 leu2Δ0 met15Δ0 ura3Δ0, NHP6a-iRFP-kanMX, pTEFmut7-CggR_R250A-CggRO-YFP::HIS3</i>
NH1843	<i>BY4741 MATa his3Δ1 leu2Δ0 met15Δ0 ura3Δ0, NHP6a-iRFP-kanMX, HXK1-GFP::HIS3</i>

7 **Table S1. Strains used or constructed in this study.** All strains will be available upon request.

8

9

Plasmid Name	Description	
NHB0638	pRS303- <i>pSIR2-SIR2</i>	10
NHB1222	pRS303- <i>pTEF1-iATPSnFR1.0</i>	11
NHB1227	pRS303- <i>TEFmu7-CggR250-CggRO</i>	12

13 **Table S2. Plasmids constructed in this study.** All plasmids will be available upon request.

14

15

Primer	Sequence (5'-3')	Description
M13@pTEF1	GTAAAACGACCGCCAGTCCACAC ACCATAGCTTCAAAAT	Forward primer to PCR TEF1 promoter for making NHB1222

ATPs@pTEF1	ATGAATAGTTTTTCATCTTAGATTA GATTGCTATGCTTTCT	Reverse primer to PCR TEF1 promoter for making NHB1222
pTEF1@ATPs	AATCTAATCTAAGATGAAAATA TTCATGTTTCTGTTGTT	Forward primer to PCR iATPSnFR1.0 for making NHB1222
M13r@ATP	AAACAGCTATGACTTAATCAACTT GCAATTTTCATT	Reverse primer to PCR iATPSnFR1.0 for making NHB1222
ATP@M13r	TGCAAGTTGATTAAGTCATAGCTG TTTCCTGTGTG	Forward primer to PCR pRS303 plasmid for making NHB1222
pTEF1@M13	ATGGTGTGTGGACTGGCCGTCGTT TTACAAC	Reverse primer to PCR pRS303 plasmid for making NHB1222
303His-I-F	ACGACCATCACACCACTGAA	Forward primer to check integration of pTEF1-iATPSnFR1.0 into genomic HIS3 location
ATP-I-R	CAGCCAATTGCATAGAACCA	Reverse primer to check integration of pTEF1-iATPSnFR1.0 into genomic HIS3 location
BamHI-CggRO-F	CGGGATCCCTGTCGATTCGATACT AACGCCG	Forward primer to PCR CggRO for making NHB1227
EcoRI-CggRO-R	GGAATTCCGAGCTGTACAAGTAG CGTTG	Reverse primer to PCR CggRO for making NHB1227
XhoI-pTEF7-CggR-F	CCGCTCGAGGCGTCGTACGCTAG GTCGAG	Forward primer to PCR pTEF7-CggR for making NHB1227
EcoRI-pTEF7-CggR-R	GGAATTCTCATTCATCTCTCAACA ACTTTTTGGC	Reverse primer to PCR pTEF7-CggR for making NHB1227
HXT1-t-F	TGATGACCAACCATTTTACAAGA GTTTGTGTTAGCAGGAAA GGTGACGGTGCTGGTTTA	Forward primer for tagging Hxt1 with fluorescence protein, using pKT series plasmid as template
HXT1-t-R	ATAAGTCATTAATAATATGCATATT GAGCTTGTTTAGTTTA TCGATGAATTCGAGCTCG	Reverse primer for tagging Hxt1 with fluorescence protein, using pKT series plasmid as template
HXT1-S-F	TCAGCTTCCTGGGTCCAGTATC	Forward primer to check HXT1-CFP tagging
HXT1-S-R	TGTTGAAGCAGCAGCGTTGT	Reverse primer to check HXT1-CFP tagging
HXT2 tag F	TGGTAGCTGGATCTCAAAAGAAA AAAGAGTTTCCGAGGAA GGTGACGGTGCTGGTTTA	Forward primer for tagging Hxt2 with fluorescence protein, using pKT series plasmid as template
HXT2 tag R	AGCCTTAAAAAATCAGTGCTAG TTTAAGTATAATCTCTTA TCGATGAATTCGAGCTCG	Reverse primer for tagging Hxt2 with fluorescence protein, using pKT series plasmid as template

HXT2 Seq F	GGTGTCAAACCATGGAAATCTG	Forward primer to check HXT2-YFP tagging
HXT2 Seq R	ACGTCGAGTCCGTAAGATTTGATC	Reverse primer to check HXT2-YFP tagging
HXT3 tag F	TGATGACCAGCCATTCTACAAGA AAATGTTTCGGCAAGAAAGGTGAC GGTGCTGGTTTA	Forward primer for tagging Hxt3 with fluorescence protein, using pKT series plasmid as template
HXT3 tag R	AATACACTATTATTCAGCACTACG GTTTAGCGTGAAATTATCGATGAA TTCGAGCTCG	Reverse primer for tagging Hxt3 with fluorescence protein, using pKT series plasmid as template
HXT3 seq F	TGCTAACTACGATGCTGATG	Forward primer to check HXT3-mCherry tagging
HXT3 seq R	ATTGACTAGCACATCGAATC	Reverse primer to check HXT3-mCherry tagging
HXK1 tag F	AAGAATTGCCGAAGGTAAGTCTC TTGGTATCATTGGCGCT- GGTGACGGTGCTGGTTTA	Forward primer for tagging Hxk1 with fluorescence protein, using pKT series plasmid as template
HXK1 tag R	GGGAAAAACACATTTATATTTTCAT TACATTTTTTTCATTATCGATGAA TTCGAGCTCG	Reverse primer for tagging Hxk1 with fluorescence protein, using pKT series plasmid as template
HXK1 seq F	ACGATTGTTCCAGCTGAGGA	Forward primer to check HXK1-GFP tagging
HXK1 seq R	AACATAAGGGCATCACTCAT	Reverse primer to check HXK1-GFP tagging

1

2 **Table S3. Primers used in this study.**

3

Parameter	Value
α_1	1 h^{-1}
α_2	1 h^{-1}
β_1	0.01 h^{-1}
β_2	0.01 h^{-1}
K_S	0.52
K_H	0.62
d_S	0.1 h^{-1}

d_H	0.3 h^{-1}
γ_1	1
γ_2	1
n_1	3
n_2	3
k_{S1}	0
k_{S2}	-0.15
k_{S3}	-0.007
k_{S4}	-0.03
b_{S1}	1.65
b_{S2}	1.66
b_{S3}	1.59
b_{S4}	1.64
k_{H1}	-0.87
k_{H2}	-0.32
k_{H3}	-0.03
k_{H4}	-0.085
b_{H1}	2.13
b_{H2}	2.07
b_{H3}	1.93
b_{H4}	2.03
ϵ_H	0.32
ϵ_S	0.32
ϵ_ψ	0.35

η	0.005
S_0	0.49
H_0	0.86
σ_S	0.05
σ_H	0.05

1

2 **Table S4. Parameters used in both deterministic and stochastic models.**

3

1 References

- 2 Al-Regaiey, K.A. (2016). The effects of calorie restriction on aging: a brief review. *Eur Rev Med*
3 *Pharmacol Sci* 20, 2468-2473.
- 4 Anderson, R.M., Bitterman, K.J., Wood, J.G., Medvedik, O., and Sinclair, D.A. (2003).
5 Nicotinamide and PNC1 govern lifespan extension by calorie restriction in *Saccharomyces*
6 *cerevisiae*. *Nature* 423, 181-185.
- 7 Arslan-Ergul, A., Ozdemir, A.T., and Adams, M.M. (2013). Aging, neurogenesis, and caloric
8 restriction in different model organisms. *Aging Dis* 4, 221-232.
- 9 Azzu, V., and Valencak, T.G. (2017). Energy Metabolism and Ageing in the Mouse: A Mini-Review.
10 *Gerontology* 63, 327-336.
- 11 Bartke, A., Brannan, S., Hascup, E., Hascup, K., and Darcy, J. (2021). Energy Metabolism and
12 Aging. *World J Mens Health* 39, 222-232.
- 13 Barzilai, N., Crandall, J.P., Kritchevsky, S.B., and Espeland, M.A. (2016). Metformin as a Tool to
14 Target Aging. *Cell Metab* 23, 1060-1065.
- 15 Belinchon, M.M., and Gancedo, J.M. (2007). Glucose controls multiple processes in
16 *Saccharomyces cerevisiae* through diverse combinations of signaling pathways. *FEMS Yeast*
17 *Res* 7, 808-818.
- 18 Blackburn, J.A.S., H. J. T.; Gro/nbech-Jensen, N. (1992). Stability and Hopf bifurcations in an
19 inverted pendulum. *American Journal of Physics*, 903–908.
- 20 Buschlen, S., Amillet, J.M., Guiard, B., Fournier, A., Marcireau, C., and Bolotin-Fukuhara, M.
21 (2003). The *S. Cerevisiae* HAP complex, a key regulator of mitochondrial function, coordinates
22 nuclear and mitochondrial gene expression. *Comp Funct Genomics* 4, 37-46.
- 23 DeRisi, J.L., Iyer, V.R., and Brown, P.O. (1997). Exploring the metabolic and genetic control of
24 gene expression on a genomic scale. *Science* 278, 680-686.
- 25 Filonov, G.S., Piatkevich, K.D., Ting, L.M., Zhang, J., Kim, K., and Verkhusha, V.V. (2011). Bright
26 and stable near-infrared fluorescent protein for in vivo imaging. *Nat Biotechnol* 29, 757-761.
- 27 Fontana, L., and Partridge, L. (2015). Promoting health and longevity through diet: from model
28 organisms to humans. *Cell* 161, 106-118.
- 29 Fontana, L., Partridge, L., and Longo, V.D. (2010). Extending healthy life span--from yeast to
30 humans. *Science* 328, 321-326.
- 31 Forsburg, S.L., and Guarente, L. (1989). Identification and characterization of HAP4: a third
32 component of the CCAAT-bound HAP2/HAP3 heteromer. *Genes Dev* 3, 1166-1178.
- 33 Gartenberg, M.R., and Smith, J.S. (2016). The Nuts and Bolts of Transcriptionally Silent
34 Chromatin in *Saccharomyces cerevisiae*. *Genetics* 203, 1563-1599.
- 35 Guarente, L., and Kenyon, C. (2000). Genetic pathways that regulate ageing in model organisms.
36 *Nature* 408, 255-262.
- 37 Hansen, A.S., Hao, N., and O'Shea, E.K. (2015). High-throughput microfluidics to control and
38 measure signaling dynamics in single yeast cells. *Nat Protoc* 10, 1181-1197.
- 39 Hersen, P., McClean, M.N., Mahadevan, L., and Ramanathan, S. (2008). Signal processing by
40 the HOG MAP kinase pathway. *Proc Natl Acad Sci U S A* 105, 7165-7170.
- 41 Hughes, A.L., and Gottschling, D.E. (2012). An early age increase in vacuolar pH limits
42 mitochondrial function and lifespan in yeast. *Nature* 492, 261-265.
- 43 Hwangbo, D.S., Lee, H.Y., Abozaid, L.S., and Min, K.J. (2020). Mechanisms of Lifespan
44 Regulation by Calorie Restriction and Intermittent Fasting in Model Organisms. *Nutrients* 12.
- 45 Jazwinski, S.M. (2002). Growing old: metabolic control and yeast aging. *Annu Rev Microbiol* 56,
46 769-792.
- 47 Jin, M., Li, Y., O'Laughlin, R., Bittihn, P., Pillus, L., Tsimring, L.S., Hasty, J., and Hao, N. (2019).
48 Divergent Aging of Isogenic Yeast Cells Revealed through Single-Cell Phenotypic Dynamics. *Cell*
49 *Syst* 8, 242-253 e243.

- 1 Johnston, M. (1999). Feasting, fasting and fermenting. Glucose sensing in yeast and other cells.
- 2 Trends Genet 15, 29-33.
- 3 Kaeberlein, M., and Kennedy, B.K. (2005). Large-scale identification in yeast of conserved ageing
- 4 genes. Mech Ageing Dev 126, 17-21.
- 5 Kaeberlein, M., McVey, M., and Guarente, L. (1999). The SIR2/3/4 complex and SIR2 alone
- 6 promote longevity in *Saccharomyces cerevisiae* by two different mechanisms. Genes Dev 13,
- 7 2570-2580.
- 8 Karin, O., Agrawal, A., Porat, Z., Krizhanovsky, V., and Alon, U. (2019). Senescent cell turnover
- 9 slows with age providing an explanation for the Gompertz law. Nat Commun 10, 5495.
- 10 Kennedy, B.K., Berger, S.L., Brunet, A., Campisi, J., Cuervo, A.M., Epel, E.S., Franceschi, C.,
- 11 Lithgow, G.J., Morimoto, R.I., Pessin, J.E., *et al.* (2014). Geroscience: linking aging to chronic
- 12 disease. Cell 159, 709-713.
- 13 Kenyon, C.J. (2010). The genetics of ageing. Nature 464, 504-512.
- 14 Kuningas, M., Mooijaart, S.P., van Heemst, D., Zwaan, B.J., Slagboom, P.E., and Westendorp,
- 15 R.G. (2008). Genes encoding longevity: from model organisms to humans. Aging Cell 7, 270-280.
- 16 Leupold, S., Hubmann, G., Litsios, A., Meinema, A.C., Takhaviev, V., Papagiannakis, A., Niebel,
- 17 B., Janssens, G., Siegel, D., and Heinemann, M. (2019). *Saccharomyces cerevisiae* goes through
- 18 distinct metabolic phases during its replicative lifespan. Elife 8.
- 19 Li, Y., Daniel, M., and Tollefsbol, T.O. (2011). Epigenetic regulation of caloric restriction in aging.
- 20 BMC Med 9, 98.
- 21 Li, Y., Jiang, Y., Paxman, J., O'Laughlin, R., Klepin, S., Zhu, Y., Pillus, L., Tsimring, L.S., Hasty,
- 22 J., and Hao, N. (2020). A programmable fate decision landscape underlies single-cell aging in
- 23 yeast. Science 369, 325-329.
- 24 Li, Y., Jin, M., O'Laughlin, R., Bittihn, P., Tsimring, L.S., Pillus, L., Hasty, J., and Hao, N. (2017).
- 25 Multigenerational silencing dynamics control cell aging. Proc Natl Acad Sci U S A 114, 11253-
- 26 11258.
- 27 Liang, Y., Liu, C., Lu, M., Dong, Q., Wang, Z., Wang, Z., Xiong, W., Zhang, N., Zhou, J., Liu, Q.,
- 28 *et al.* (2018). Calorie restriction is the most reasonable anti-ageing intervention: a meta-analysis
- 29 of survival curves. Sci Rep 8, 5779.
- 30 Liew, C.W., Rand, K.D., Simpson, R.J., Yung, W.W., Mansfield, R.E., Crossley, M., Proetorius-
- 31 Ibba, M., Nerlov, C., Poulsen, F.M., and Mackay, J.P. (2006). Molecular analysis of the interaction
- 32 between the hematopoietic master transcription factors GATA-1 and PU.1. J Biol Chem 281,
- 33 28296-28306.
- 34 Lin, S.J., Kaeberlein, M., Andalis, A.A., Sturtz, L.A., Defossez, P.A., Culotta, V.C., Fink, G.R., and
- 35 Guarente, L. (2002). Calorie restriction extends *Saccharomyces cerevisiae* lifespan by increasing
- 36 respiration. Nature 418, 344-348.
- 37 Lobas, M.A., Tao, R., Nagai, J., Kronschlager, M.T., Borden, P.M., Marvin, J.S., Looger, L.L., and
- 38 Khakh, B.S. (2019). A genetically encoded single-wavelength sensor for imaging cytosolic and
- 39 cell surface ATP. Nat Commun 10, 711.
- 40 Longo, V.D., and Panda, S. (2016). Fasting, Circadian Rhythms, and Time-Restricted Feeding in
- 41 Healthy Lifespan. Cell Metab 23, 1048-1059.
- 42 Lopez-Otin, C., Blasco, M.A., Partridge, L., Serrano, M., and Kroemer, G. (2013). The hallmarks
- 43 of aging. Cell 153, 1194-1217.
- 44 Madeo, F., Carmona-Gutierrez, D., Hofer, S.J., and Kroemer, G. (2019). Caloric Restriction
- 45 Mimetics against Age-Associated Disease: Targets, Mechanisms, and Therapeutic Potential. Cell
- 46 Metab 29, 592-610.
- 47 Madeo, F., Carmona-Gutierrez, D., Kepp, O., and Kroemer, G. (2018). Spermidine delays aging
- 48 in humans. Aging (Albany NY) 10, 2209-2211.
- 49 Mahmoudi, S., and Brunet, A. (2012). Aging and reprogramming: a two-way street. Curr Opin Cell
- 50 Biol 24, 744-756.

- 1 Martel, J., Chang, S.H., Wu, C.Y., Peng, H.H., Hwang, T.L., Ko, Y.F., Young, J.D., and Ojcius,
2 D.M. (2021). Recent advances in the field of caloric restriction mimetics and anti-aging molecules.
3 *Ageing Res Rev* 66, 101240.
- 4 Mattson, M.P., Longo, V.D., and Harvie, M. (2017). Impact of intermittent fasting on health and
5 disease processes. *Ageing Res Rev* 39, 46-58.
- 6 McCormick, M.A., Delaney, J.R., Tsuchiya, M., Tsuchiyama, S., Shemorry, A., Sim, S., Chou,
7 A.C., Ahmed, U., Carr, D., Murakami, C.J., *et al.* (2015). A Comprehensive Analysis of Replicative
8 Lifespan in 4,698 Single-Gene Deletion Strains Uncovers Conserved Mechanisms of Aging. *Cell*
9 *Metab* 22, 895-906.
- 10 McMurray, M.A., and Gottschling, D.E. (2004). Aging and genetic instability in yeast. *Curr Opin*
11 *Microbiol* 7, 673-679.
- 12 Medvedik, O., Lamming, D.W., Kim, K.D., and Sinclair, D.A. (2007). MSN2 and MSN4 link calorie
13 restriction and TOR to sirtuin-mediated lifespan extension in *Saccharomyces cerevisiae*. *PLoS*
14 *Biol* 5, e261.
- 15 Melzer, D., Pilling, L.C., and Ferrucci, L. (2020). The genetics of human ageing. *Nat Rev Genet*
16 21, 88-101.
- 17 Miller, R.A., Harrison, D.E., Astle, C.M., Baur, J.A., Boyd, A.R., de Cabo, R., Fernandez, E.,
18 Flurkey, K., Javors, M.A., Nelson, J.F., *et al.* (2011). Rapamycin, but not resveratrol or simvastatin,
19 extends life span of genetically heterogeneous mice. *J Gerontol A Biol Sci Med Sci* 66, 191-201.
- 20 Mohammed, I., Hollenberg, M.D., Ding, H., and Triggle, C.R. (2021). A Critical Review of the
21 Evidence That Metformin Is a Putative Anti-Aging Drug That Enhances Healthspan and Extends
22 Lifespan. *Front Endocrinol (Lausanne)* 12, 718942.
- 23 Monteiro, F., Hubmann, G., Takhaveev, V., Vedelaar, S.R., Norder, J., Hekelaar, J., Saldida, J.,
24 Litsios, A., Wijma, H.J., Schmidt, A., *et al.* (2019). Measuring glycolytic flux in single yeast cells
25 with an orthogonal synthetic biosensor. *Mol Syst Biol* 15, e9071.
- 26 Niwa, H., Toyooka, Y., Shimosato, D., Strumpf, D., Takahashi, K., Yagi, R., and Rossant, J. (2005).
27 Interaction between Oct3/4 and Cdx2 determines trophectoderm differentiation. *Cell* 123, 917-
28 929.
- 29 Novelle, M.G., Ali, A., Dieguez, C., Bernier, M., and de Cabo, R. (2016). Metformin: A Hopeful
30 Promise in Aging Research. *Cold Spring Harb Perspect Med* 6, a025932.
- 31 O'Laughlin, R., Jin, M., Li, Y., Pillus, L., Tsimring, L.S., Hasty, J., and Hao, N. (2020). Advances
32 in quantitative biology methods for studying replicative aging in *Saccharomyces cerevisiae*. *Transl*
33 *Med Aging* 4, 151-160.
- 34 Ozcan, S., and Johnston, M. (1999). Function and regulation of yeast hexose transporters.
35 *Microbiol Mol Biol Rev* 63, 554-569.
- 36 Paxman, J., Zhou, Z., O'Laughlin, R., Liu, Y., Li, Y., Tian, W., Su, H., Jiang, Y., Holness, S.E.,
37 Stasiowski, E., *et al.* (2022). Age-dependent aggregation of ribosomal RNA-binding proteins links
38 deterioration in chromatin stability with challenges to proteostasis. *Elife* 11.
- 39 Petr, M.A., Alfaras, I., Krawczyk, M., Bair, W.N., Mitchell, S.J., Morrell, C.H., Studenski, S.A.,
40 Price, N.L., Fishbein, K.W., Spencer, R.G., *et al.* (2021). A cross-sectional study of functional and
41 metabolic changes during aging through the lifespan in male mice. *Elife* 10.
- 42 Ravera, S., Podesta, M., Sabatini, F., Dagnino, M., Cilloni, D., Fiorini, S., Barla, A., and Frassoni,
43 F. (2019). Discrete Changes in Glucose Metabolism Define Aging. *Sci Rep* 9, 10347.
- 44 Roberts, S.B., and Rosenberg, I. (2006). Nutrition and aging: changes in the regulation of energy
45 metabolism with aging. *Physiol Rev* 86, 651-667.
- 46 Rolland, F., Winderickx, J., and Thevelein, J.M. (2002). Glucose-sensing and -signalling
47 mechanisms in yeast. *FEMS Yeast Res* 2, 183-201.
- 48 Saka, K., Ide, S., Ganley, A.R., and Kobayashi, T. (2013). Cellular senescence in yeast is
49 regulated by rDNA noncoding transcription. *Curr Biol* 23, 1794-1798.
- 50 Selvarani, R., Mohammed, S., and Richardson, A. (2021). Effect of rapamycin on aging and age-
51 related diseases-past and future. *Geroscience* 43, 1135-1158.

- 1 Shu, J., Wu, C., Wu, Y., Li, Z., Shao, S., Zhao, W., Tang, X., Yang, H., Shen, L., Zuo, X., *et al.*
- 2 (2013). Induction of pluripotency in mouse somatic cells with lineage specifiers. *Cell* *153*, 963-
- 3 975.
- 4 Sinclair, D.A., and Guarente, L. (1997). Extrachromosomal rDNA circles--a cause of aging in
- 5 yeast. *Cell* *91*, 1033-1042.
- 6 Sinclair, D.A., Mills, K., and Guarente, L. (1997). Accelerated aging and nucleolar fragmentation
- 7 in yeast *sgs1* mutants. *Science* *277*, 1313-1316.
- 8 Taormina, G., and Mirisola, M.G. (2014). Calorie restriction in mammals and simple model
- 9 organisms. *Biomed Res Int* *2014*, 308690.
- 10 Vijg, J., and Suh, Y. (2013). Genome instability and aging. *Annu Rev Physiol* *75*, 645-668.
- 11 Westholm, J.O., Nordberg, N., Muren, E., Ameer, A., Komorowski, J., and Ronne, H. (2008).
- 12 Combinatorial control of gene expression by the three yeast repressors Mig1, Mig2 and Mig3.
- 13 *BMC Genomics* *9*, 601.
- 14 Yang, Y., Karin, O., Mayo, A., Song, X., Chen, P., Santos, A.L., Lindner, A.B., and Alon, U. (2023).
- 15 Damage dynamics and the role of chance in the timing of *E. coli* cell death. *Nat Commun* *14*,
- 16 2209.
- 17 Zhang, T., Bu, P., Zeng, J., and Vancura, A. (2017). Increased heme synthesis in yeast induces
- 18 a metabolic switch from fermentation to respiration even under conditions of glucose repression.
- 19 *J Biol Chem* *292*, 16942-16954.
- 20 Zhou, Z., Liu, Y., Feng, Y., Klepin, S., Tsimring, L.S., Pillus, L., Hasty, J., and Hao, N. (2023).
- 21 Engineering longevity-design of a synthetic gene oscillator to slow cellular aging. *Science* *380*,
- 22 376-381.
- 23

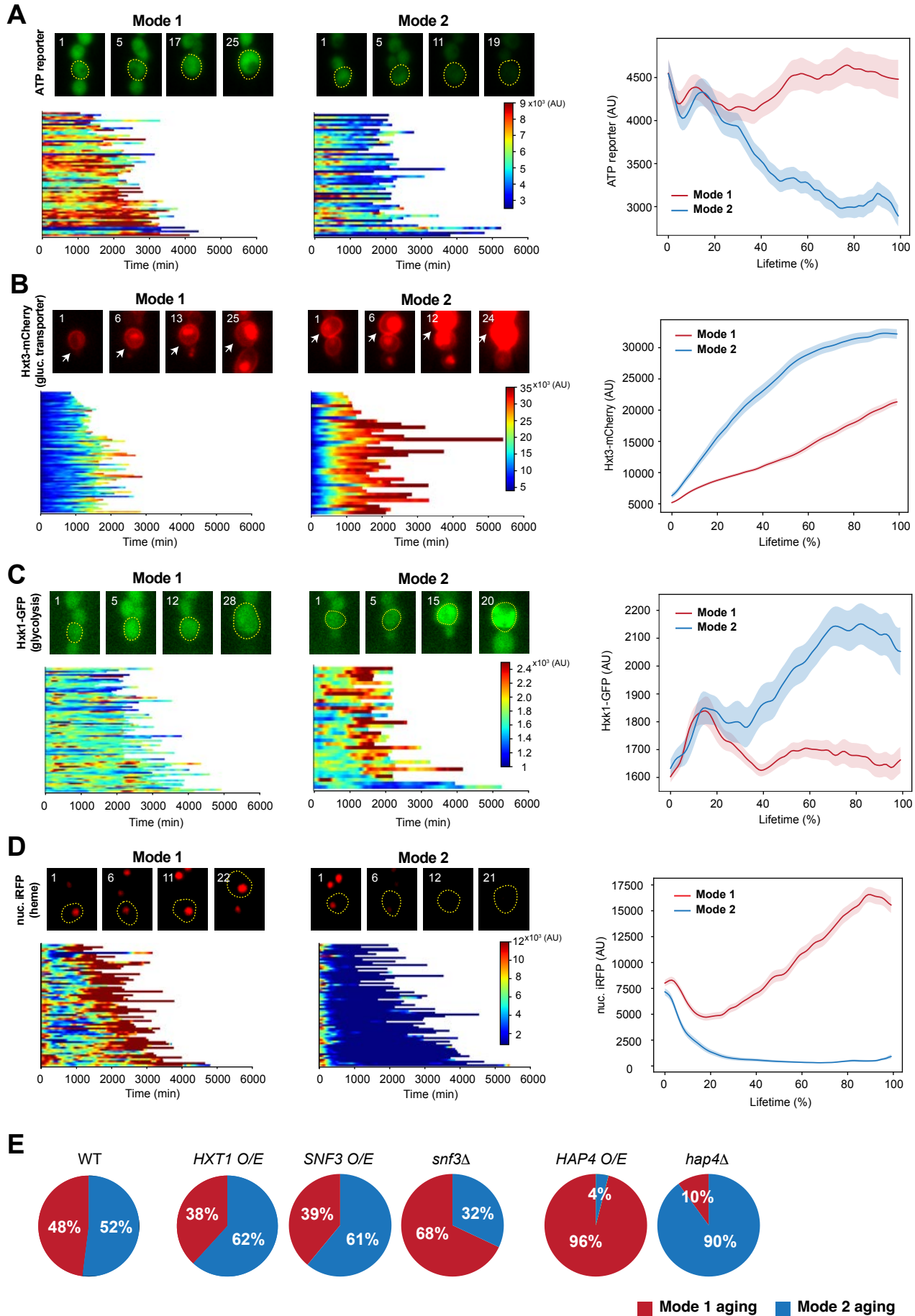


Fig.1

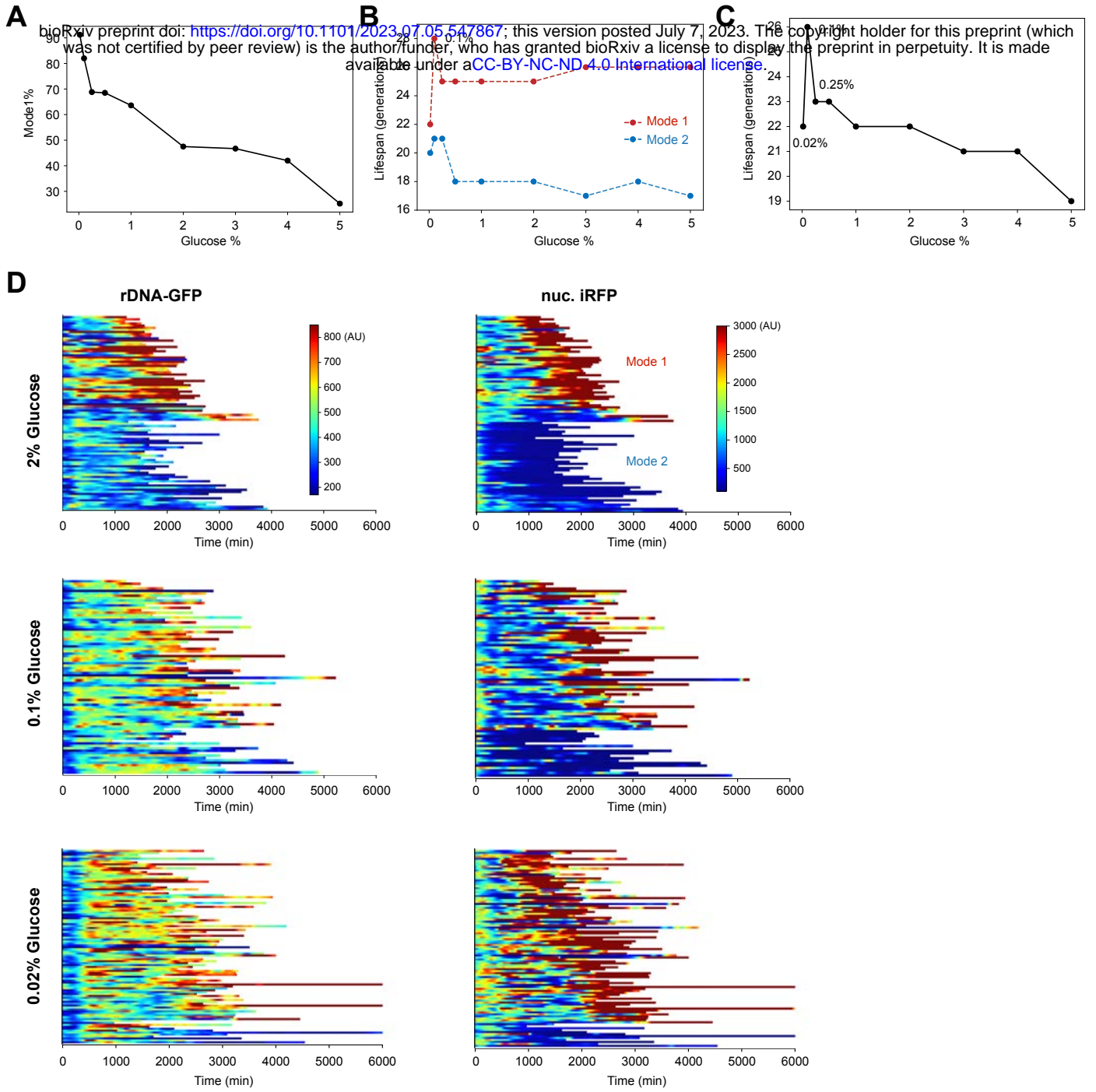


Fig.2

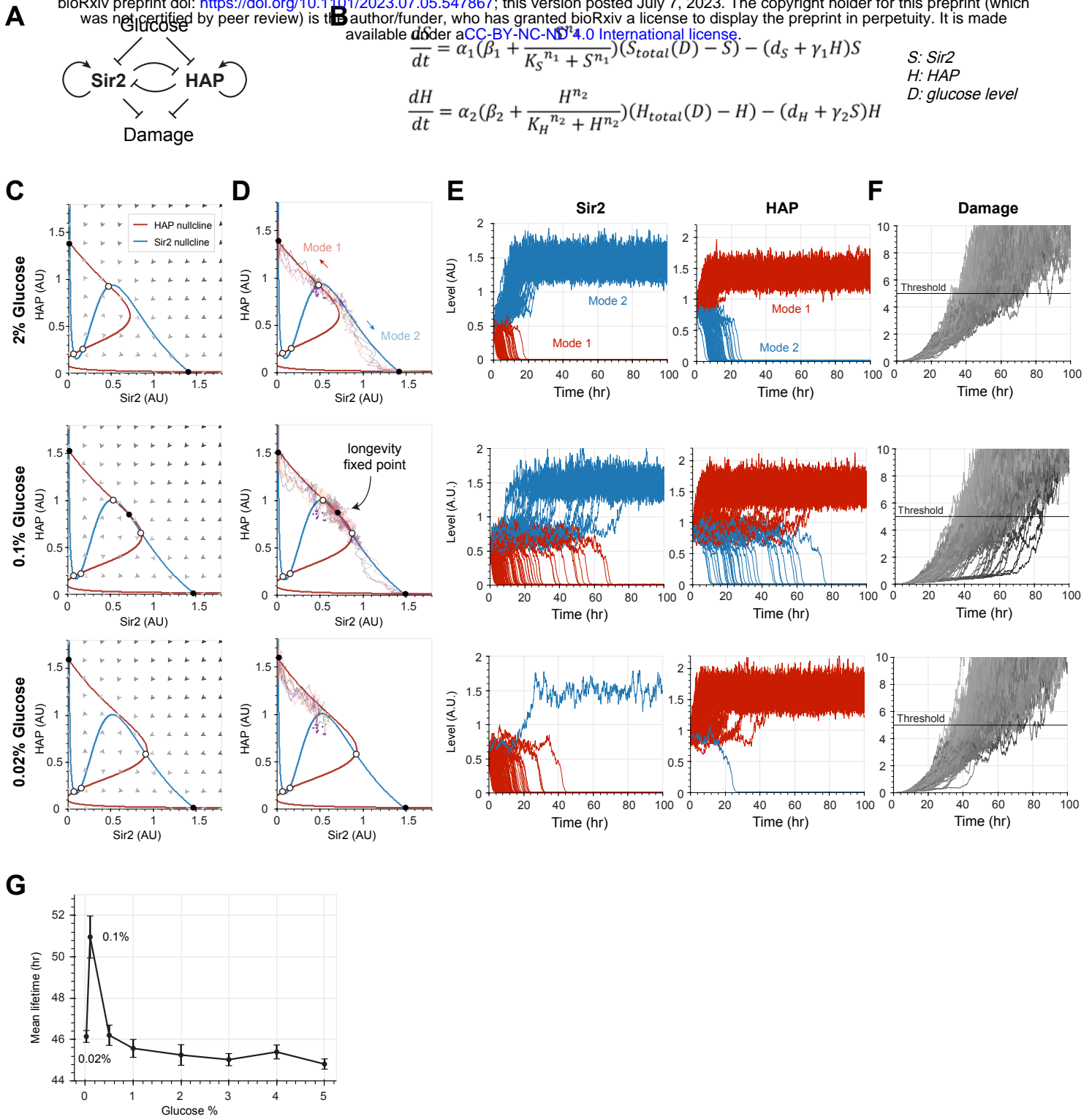


Fig.3

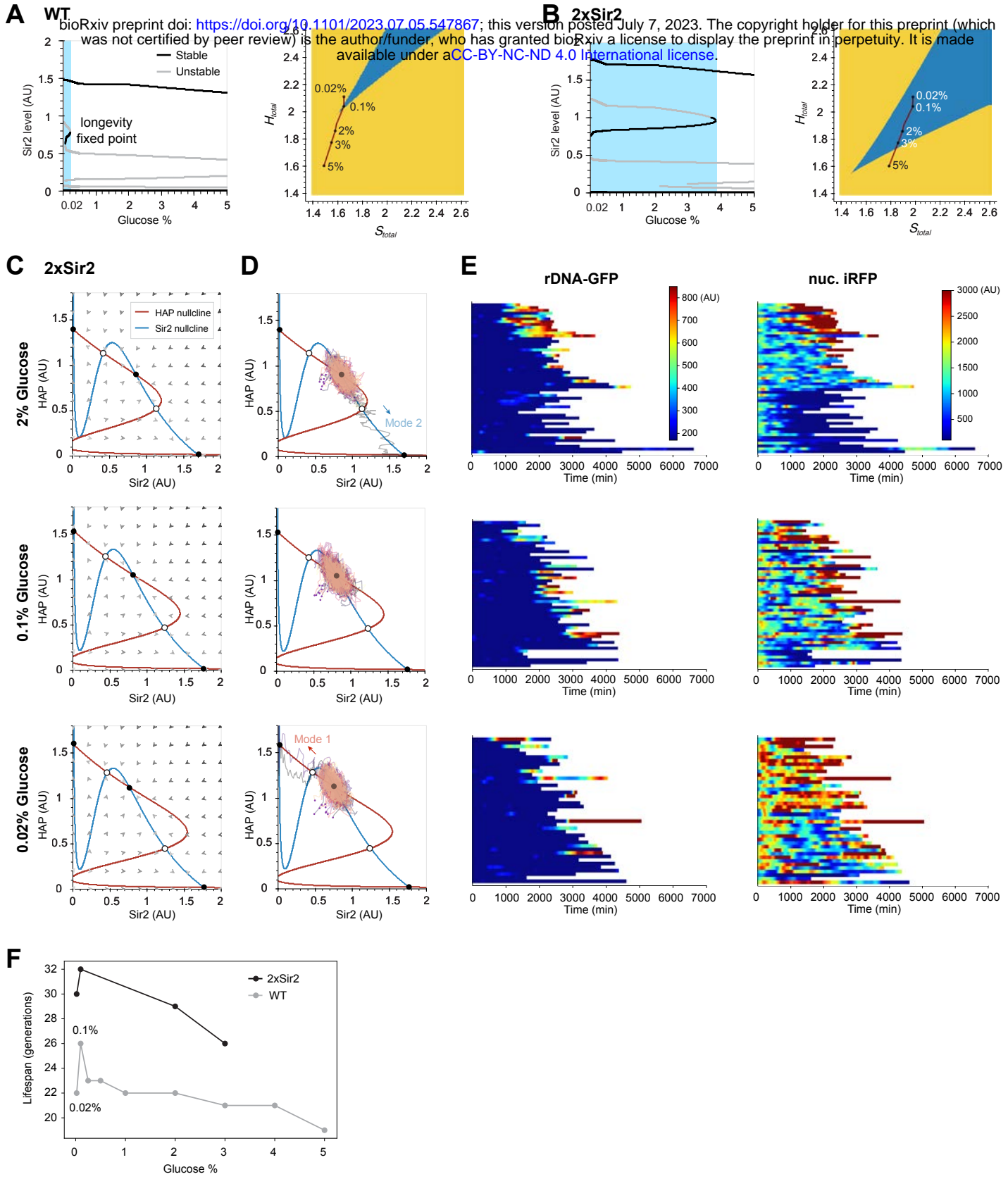


Fig.4

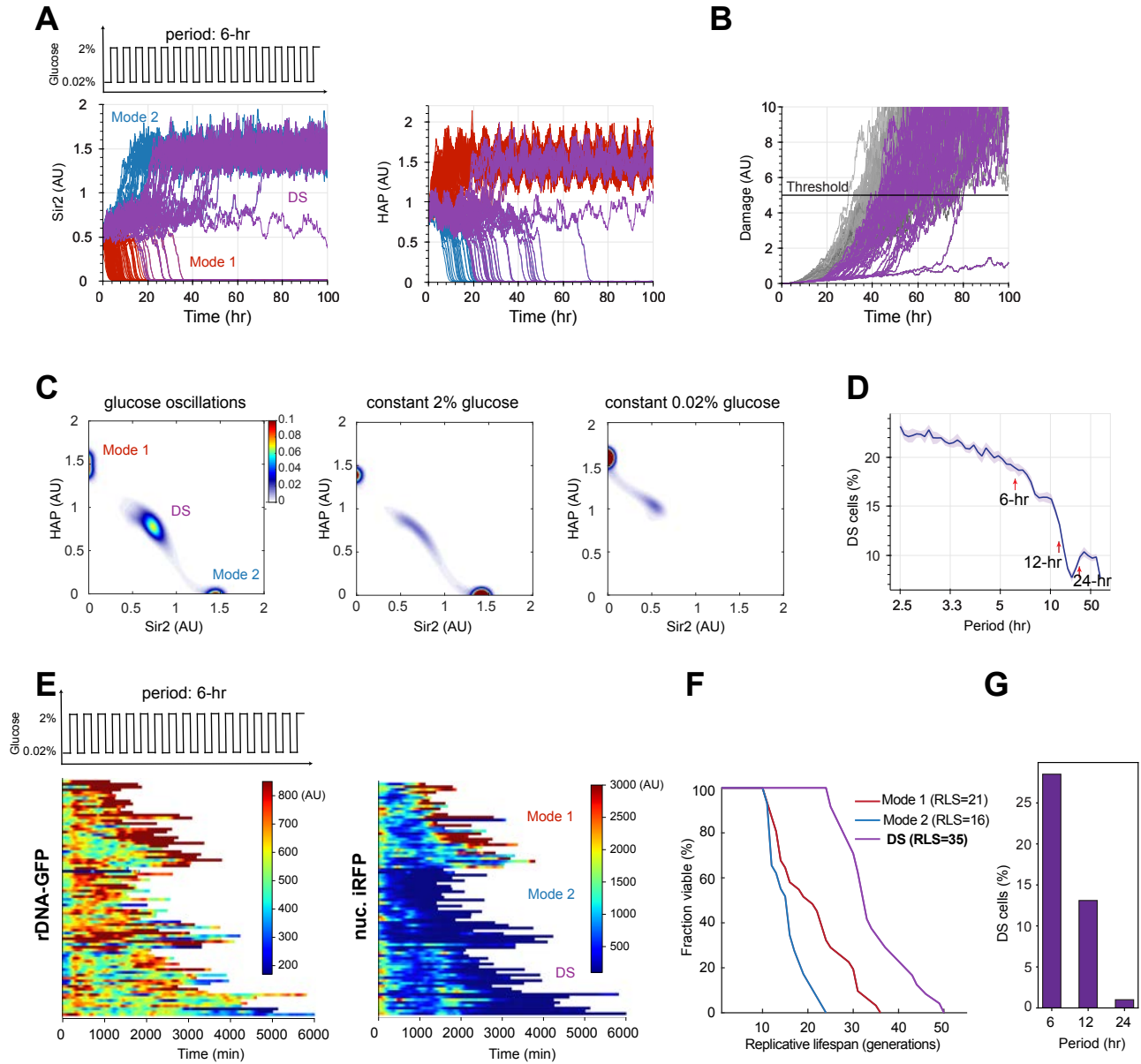


Fig.5